Bioconjugate Chemistry

Article

pubs.acs.org/bc

In Vivo Type 2 Cannabinoid Receptor-Targeted Tumor Optical Imaging Using a Near Infrared Fluorescent Probe

Shaojuan Zhang,[†,‡,∥] Pin Shao,[†,∥] and Mingfeng Bai*[,†,§]

[†]Molecular Imaging Laboratory, Department of Radiology, University of Pittsburgh, Pittsburgh, Pennsylvania 15219, United States
[‡]Department of Diagnostic Radiology, the First Hospital of Medical School, Xi'an Jiaotong University, Xi'an, Shaanxi 710061, China
[§]University of Pittsburgh Cancer Institute, Pittsburgh, Pennsylvania 15232, United States

Supporting Information

ABSTRACT: The type 2 cannabinoid receptor (CB_2R) plays a vital role in carcinogenesis and progression and is emerging as a therapeutic target for cancers. However, the exact role of CB_2R in cancer progression and therapy remains unclear. This has driven the increasing efforts to study CB_2R and cancers using molecular imaging tools. In addition, many types of cancers overexpress CB_2R, and the expression levels of CB_2R appear to be associated with tumor aggressiveness. Such upregulation of the receptor in cancer cells provides opportunities for CB_2R-targeted imaging with high contrast and for therapy with low side effects. In the present study, we report the first in vivo tumor-targeted optical imaging using a novel CB_2R-targeted near-infrared probe. In vitro cell fluorescent imaging and a competitive binding assay indicated specific binding of NIR760-mbc94 to CB_2R in CB_2-mid delayed brain tumor (DBT) cells. NIR760-mbc94 also preferentially labeled CB_2-mid DBT tumors in vivo, with a 3.7-fold tumor-to-normal contrast enhancement at 72 h postinjection, whereas the fluorescence signal from the tumors of the mice treated with NIR760 free dye was nearly at the background level at the same time point. SR144528, a CB_2R competitor, significantly inhibited tumor uptake of NIR760-mbc94, indicating that NIR760-mbc94 binds to CB_2R specifically. In summary, NIR760-mbc94 specifically binds to CB_2R in vitro and in vivo and appears to be a promising molecular tool that may have great potential for use in diagnostic imaging of CB_2R-positive cancers and therapeutic monitoring as well as in elucidating the role of CB_2R in cancer progression and therapy.

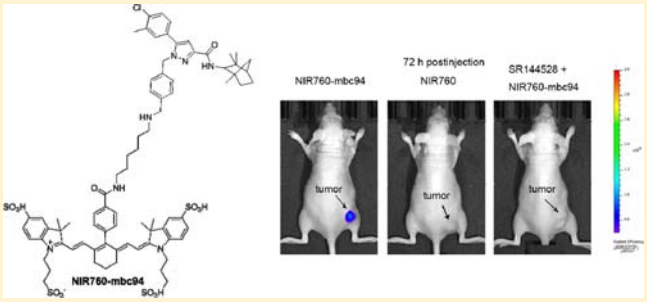

INTRODUCTION

Cannabinoid receptors belong to the G protein-coupled receptor (GPCR) family and are involved in the regulation of fundamental cellular functions throughout the body.[1] To date, two types of cannabinoid receptors, type 1 (CB_1R) and type 2 (CB_2R), have been cloned and characterized.[2] In general, CB_1R is expressed at high levels in the brain and at much lower levels in peripheral tissues, whereas CB_2R is predominantly a peripheral receptor abundantly expressed by immune cells.[3,4] Recent studies have shown that CB_2R plays a vital role in cancer evolution and progression and that CB_2R ligands may offer therapeutic potential for cancer treatment.[5,6] However, the exact role of CB_2R in cancer remains unclear. This has driven the increasing efforts to study CB_2R and cancers using molecular imaging tools.

CB_2R represents a unique type of target for cancer research. CB_2R expression is high only in the spleen, tonsils, thymus, macrophages, and leucocytes, and it is low or even undetectable in the brain, thyroid, retina, placenta, skeletal muscle, kidney, liver, adrenal gland, heart, prostate, and ovary.[7,8] However, many types of cancers overexpress CB_2R, such as prostate, skin, liver, and breast cancers, and the expression levels of CB_2R appear to be associated with tumor aggressiveness.[9−13] Such upregulation of the receptor in cancer cells provides opportunities for CB_2R-targeted imaging with high contrast and for therapy with low side effects. However, the field of CB_2R-targeted imaging, particularly in oncology, is largely unexplored.

To date, only a limited number of CB_2R-targeted contrast agents have been reported for noninvasive positron emission tomography (PET) imaging of CB_2R in cancers,[14−17] and few studies have been reported with other imaging modalities, such as magnetic resonance imaging (MRI), optical imaging, and ultrasound.[18] Despite the advantages of high sensitivity and deep tissue penetration, PET has many limitations, such as relatively low resolution, narrow time window, high instrument cost, and injection of radioactive agents. Optical imaging, however, serves as an alternative low-cost approach with relatively high sensitivity and resolution. The major disadvantage of limited tissue penetration can be partially resolved by adapting near-infrared (NIR) light (650−900 nm), under which tissues have a relatively low absorption, scattering, and

Received: July 15, 2013
Revised: October 3, 2013
Published: October 7, 2013

autofluorescence.[19] As such, NIR optical imaging is suitable for both cellular and in vivo imaging applications.

Recently, we reported the first NIR CB_2R-targeted probe, NIR-mbc94, and validated its selective binding to CB_2R in vitro.[20] Building upon our previous study, we now report the development, in vitro characterization, and in vivo cancer imaging of a novel CB_2R-targeted NIR probe, NIR760-mbc94. To the best of our knowledge, this is the first in vivo optical imaging study using a CB_2R-targeted NIR probe. Such a probe may serve as a valuable tool to image cancers and to elucidate the role of CB_2R in cancer progression and therapy.

EXPERIMENTAL SECTION

Preparation of CB_2R-Targeted NIR Probe NIR760-mbc94. The solvents used were of commercial grade. The ligand **mbc94** was synthesized using a previously described procedure.[8] Flash column chromatography was performed on a Teledyne ISCO (combiflash RF) purification system with silica gel (standard grade, 60A, Sorbtech) or C18-reversed-phase silica gel (20−40 μm, RediSepRf). ^{1}H and ^{13}C NMR spectra were recorded on a Bruker Avance III 400 MHz. Mass spectra were recorded on a Waters LCT Premier mass spectrometer. UV−vis spectra were recorded on a Cary 100 Bio UV−vis spectrophotometer, and fluorescence spectra were recorded on a Cary Eclipse fluorescence spectrophotometer.

NIR760. The synthetic method is similar to the reported procedure.[21] Overall yield (two steps): 42%. ^{1}H NMR (DMSO-d_6): δ = 8.14 (d, 2H, J = 8 Hz), 7.55−7.58 (m, 4H), 7.32 (d, 2H, J = 8 Hz), 7.26 (d, 2H, J = 8.4 Hz), 7.09 (d, 2H, J = 14.4 Hz), 6.41 (d, 2H, J = 14.4 Hz), 4.26 (br.s, 4H), 2.71 (br.st, 4H), 2.54−2.55 (m, 4H), 1.94−1.97 (m, 6H), 1.1 (s, 12H). MS (ESI): m/z $(M + 3H)^+$ calcd for $C_{43}H_{48}N_2O_{14}S_4$, 944.20; found, 944.44.

NIR760-mbc94. A mixture of NIR760 (10 mg, 10 μmol), HBTU (5 mg, 13 μmol), and HOBt (1.8 mg, 13 μmol) in dry DMF (2 mL) was stirred at room temperature for 5 min. DIEA (3 μL, 17 μmol) was then added, and the mixture was stirred for another 10 min. After that, mbc94 (6 mg, 10 μmol) in dry DMF (1 mL) was added to the dye solution. The resulting mixture was stirred at room temperature under an atmosphere of Argon in the absence of light for 24 h. The solvent was removed, and the resulting solid was purified over a C18-reversed-phase silica gel column using H_2O/MeOH (20% MeOH to 75% MeOH) as eluent, resulting in NIR760-mbc94 (4 mg, 25%) as a green solid. ^{1}H NMR (DMSO-d_6): δ = 8.62 (t, 1H, J = 4.8 Hz), 8.13 (d, 2 H, J = 8 Hz), 7.59 (d, 2H, J = 8 Hz), 7.46−7.51 (m, 5H), 7.38 (d, 2H, J = 8 Hz), 7.35 (d, 2H, J = 8 Hz), 7.29 (d, 1H, J = 8 Hz), 7.09 (d, 1H, J = 9.6 Hz), 7.01−7.06 (m, 3H), 6.91 (d, 1H, J = 9.2 Hz), 6.44 (d, 2H, J = 14.4 Hz), 5.5 (s, 2H), 4.27 (m, 4H), 4.11 (s, 2H), 3.69 (d, 1H, J = 8.8 Hz), 2.9 (t, 2H, J = 7.6 Hz), 2.72 (br.s, 4H), 2.52−2.54 (m, 4H), 2.33 (s, 3H), 1.92−1.97 (m, 6H), 1.62−1.73 (m, 6H), 1.23−1.34 (m, 8H), 1.08 (s, 12H), 1.01 (s, 3H), 0.84 (t, 3H, J = 7.2 Hz), 0.78 (s, 3H). ^{13}C NMR (DMSO-d_6): δ = 171.82, 165.71, 162.04, 146.39, 144.94, 142.80, 140.44, 138.16, 136.69, 134.27, 131.87, 131.84, 131.70, 130.88, 129.80, 129.66, 128.57, 128.10, 127.37, 110.70, 63.19, 48.48, 48.47, 48.22, 48.07, 31.31, 27.56, 26.22, 25.57, 25.40, 23.76, 21.59, 20.05, 20.01, 16.96, 14.23. MS (ESI): m/z $(M + H)^+$ calcd for $C_{78}H_{95}ClN_7O_{14}S_4$, 1516.55; found, 1516.6.

Viability Assay. The cell viability assay was performed using a mouse malignant astrocytoma cell line transfected with CB_2R, CB_2-mid DBT, which expresses CB_2R at endogenous levels.[22] CB_2-mid DBT cells were cultured in DMEM containing 10% fetal bovine serum, 4 mM glutamine, 100 units/ml of penicillin, and 100 μg/mL of streptomycin. CB_2-mid DBT cells were treated with various concentrations of NIR760-mbc94 ranging from 0 to 100 μM, with indocyanine green (ICG) (Sigma-Aldrich) serving as a negative control and tamoxifen (COSH Healthcare LTD) as a positive control[23] for 24 h in a water-jacketed incubator (37 °C, 5% CO_2). Cell viability was determined by the CellTiter-Glo Luminescent Cell Viability Assay kit (Promega) as per the manufacturer's instructions.

Stability Study. To compare the stability of NIR760 and IRDye-800CW, solutions of the respective dyes in PBS with the same initial absorbance of 0.65 at the maximum absorption wavelength were kept in capped clear glass vials and exposed to ambient light. The fluorescence intensities at the maximum emission wavelength of the dyes were recorded in 1 cm quartz cuvettes (3 mL) over time.

Reverse Transcription Polymerase Chain Reaction (RT-PCR). For CB_2-mid DBT cell samples, CB_2-mid DBT cells were seeded onto 3.5 mm dishes and cultured at 37 °C for 24 h. To collect CB_2-mid DBT tumor samples, 1×10^6 CB_2-mid DBT cells were subcutaneously implanted into the right flank of a 6−8 week old female nu/nu mouse. After approximately 10 days of tumor growth, mice were sacrificed, and CB_2-mid DBT tumors were isolated and rapidly frozen by liquid nitrogen for storage. Total RNA was extracted from both CB_2-mid DBT cells and CB_2-mid DBT tumor samples using RNAzol Reagent (Invitrogen). Single-strand cDNA was synthesized from total RNA using the SuperScript III first-strand synthesis system for RT-PCR (Invitrogen). For quantitative real-time PCR assays, primers for CB_2R and GAPDH (housekeeping gene) were obtained from Integrated DNA Technologies. The sequences used for CB_2R were 5′-tcctatcatttacgccctgc-3′ and 5′-ggctcctaggtggtttttcacatcagcctc-3′,[19] and for GAPDH (as housekeeping gene), the primer sequences were 5′-tgaacgggaagctcactggcat-3′ and 5′-tgcctgcttcaccaccttcttg-3′. First-strand cDNAs were synthesized using the SuperScript III first-strand synthesis system for RT-PCR (Invitrogen). Amplifications were run using Platinum Taq DNA polymerase (Invitrogen) and consisted of 30 cycles of 30 s at 94 °C, 30 s at 55 °C, and 30 s at 72 °C.

Western Blot. CB_2-mid DBT cell and tumor samples were prepared using the same method described above. Cell lysates and tumor lysates were extracted with RIPA buffer with Halt Protease Inhibitor Cocktail (Thermo Scientific). Thirty micrograms of whole CB_2-mid DBT cell and tumor protein extracts was resolved on a 10% SDS-PAGE gel before electrophoretic transfer onto a nitrocellulose membrane. After blocking with 5% nonfat milk in TBS-T (Tris-buffered solution pH 7.6 with 0.005% Tween 20), the membranes were incubated overnight at 4 °C with anti-CB_2 primary monoclonal antibodies (Sigma-Aldrich) diluted in blocking buffer. The primary antibody reaction was followed by a 1 h incubation with the appropriate secondary antibodies. Immunocomplexes were detected using an enhanced chemiluminescence detection system and membrane exposure using the Chemi Doc MP Imaging System (Bio-Rad).

In Vitro Saturation Binding Assay of NIR760-mbc94. We carried out an intact cell saturation binding assay to determine CB_2R binding affinity to NIR760-mbc94.[24] Briefly, CB_2-mid DBT cells were seeded onto 96−well optical bottom plates and incubated for 24 h. HBSS with 1 mM Mg^{2+}, 0.1%

BSA, and 0.1% NaN_3 was used as the binding medium. Cells were preincubated with or without 100 nM of the blocking agent SR144528 (Cayman Chemical) for 30 min (nonspecific binding or total binding) and were then incubated for 1 h with an increasing concentration of NIR760-mbc94 at 4 °C. Cells were then rinsed, and fluorescence at 790 nm (relative fluorescence units, RFU) was read with a SynergyTM H4 Hybrid Multi-Mode Microplate Reader. DRAQ-5 (Cell Signaling) was used to normalize cell numbers from RFU. The specific binding was obtained by the subtraction of nonspecific binding from the total binding. The dissociation constant (K_d) and receptor density (B_{max}) were estimated from the nonlinear fitting of specific binding versus NIR760-mbc94 concentration using Prism software (GraphPad).

Cell Fluorescent Imaging of NIR760-mbc94. CB_2-mid DBT cells were treated with 5 μM NIR760-mbc94 or NIR760 at 37 °C for 30 min with or without 30 min of pretreatment with 10 μM of SR144528 as the CB_2R competitor. After washing three times with serum-free medium, the cells were fixed with 4% paraformaldehyde/PBS for 20 min at room temperature. Cells were then permeabilized with 0.1% Triton X-100. The cell nucleus was stained with 1 μg/mL of DAPI for 15 min at room temperature. Cells were mounted and then imaged using the Zeiss Axio Observer fluorescent microscope with the ApoTome 2 imaging system. NIR760-mbc94 or NIR760 fluorescent images were captured with a NIR camera under ICG filters (excitation/emission: 750−800/820−875 nm). Nuclear images were obtained with DAPI filters (excitation/emission: 335−383/420−470 nm). Differential interference contrast (DIC) images were obtained through Trans light DIC.

We used a multiplate reader system for the quantitative CB_2R binding assay. CB_2-mid DBT cells were grown to 90% confluence in T75 flasks, harvested, and seeded onto 96-well optical plates followed by incubation in a water-jacketed incubator (37 °C, 5% CO_2) for 24 h prior to the assay. On the day of the assay, the culture medium was aspirated and replaced with 100 μL of serum-free media with or without 10 μM of SR144528 for 30 min at 37 °C. Next, 5 μM NIR760-mbc94 or NIR760 or DMSO as the vehicle was added in culture medium, and the cells were incubated for an additional 30 min. Prior to reading the plate, the cells were washed three times with serum-free medium. A Synergy H4 Hybrid Multi-Mode Microplate Reader was used for reading fluorescence at 740/790 nm (excitation/emission). Assays for each group were done in triplicate.

In Vivo Optical Imaging and Competitive Blocking Studies. We conducted our animal experiments in accordance with the guidelines for the Care and Use of Laboratory Animals of the Medical Research Council of University of Pittsburgh. CB_2-mid DBT cells (1×10^6) were subcutaneously implanted into the right flank of 6−8 week old female nu/nu mice. Experiments with tumor-bearing mice were performed 10 days after the injection of tumor cells. Mice were divided into three groups, and the mice were injected with the following agents (dissolved in 100 μL of saline) via the tail vein: three mice received 10 nmol of NIR760-mbc94, three received 10 nmol of free NIR760, and three mice received 100 nmol of SR144528 that was administered 1 h before the injection of 10 nmol of NIR760-mbc94 (SR144528 + NIR760-mbc94). Mice were anesthetized with 2.5% isoflurane, and tumor CB_2R-targeted images were obtained preinjection and at 0.02, 1, 2, 6, 12, 24, 48, and 72 h postinjection with a charge-coupled device camera-based bioluminescence imaging system (IVIS Lumina XR; excitation filter, 745 nm; emission filter, 800 nm; exposure time, 1 s; binning, small; field of view, 12; f/stop, 2; open filter). The signal was displayed as radiant efficiency ([photons/s/cm^2/sr]/[μW/cm^2]). Images were acquired and analyzed using Living Image 2.5 software (Xenogen). For determining tumor contrast, the radiant efficiency of the tumor area at the right flank of the animal (T) and of the area at the left flank [normal tissue (N)] was calculated by the region of interest (ROI) function in the Living Image software. Dividing T by N yielded the contrast between the tumor and normal tissue.

Ex Vivo Imaging, Biodistribution, and Histological Study. At 72 h postinjection of NIR760-mbc94, NIR760, or SR144528 + NIR760-mbc94, CB_2-mid DBT tumor-bearing nude mice were sacrificed. Tumors as well as organs of interest (blood, heart, lung, liver, spleen, pancreas, kidney, muscle from left leg, and brain) were extracted. Ex vivo imaging was carried out, and biodistribution was analyzed. For histological study, tumor samples were embedded in Tissue-Tek OCT compound mounting medium (Sakura Finetek U.S.A. Inc.), frozen in liquid nitrogen, and cryostat-sectioned (5 μm) using a Leica Jung CM3000. Histological sections from cryostat blocks were stained with hematoxylin and eosin (H&E).

Data Processing and Statistics. All of the data are given as the mean ± standard deviation (SD) of n independent measurements. Statistical analysis was performed using a two-tailed unpaired Student's t test (IBM SPSS Statistics version 21), with p values <0.05 considered to be statistically significant.

RESULTS

Characterization of Properties of NIR760-mbc94. To develop the NIR CB_2R probe, NIR760-mbc94, we synthesized a functional CB_2R ligand, mbc94, and a NIR dye, NIR760. Mbc94 was then coupled to NIR760 using an amide-coupling reaction (Figure 1a,b). Both the free dye, NIR760, and the probe, NIR760-mbc94, show intense absorption in the NIR region in aqueous solutions (Figure 1c). NIR760 has a maximum absorption peak at 760 nm, which was red-shifted to 766 nm after mbc94 was coupled to NIR760. The molar extinction coefficients of NIR760 and NIR760-mbc94 are 2.4×10^5 and 1.44×10^5 M^{-1} cm^{-1}, respectively. NIR760 and NIR760-mbc94 are highly emissive, and they exhibit strong fluorescence with maxima at 781 and 785 nm, respectively. Their relative fluorescence quantum yields in water were measured with indocyanine green (ICG) as the standard.[21] The quantum yield of NIR760 is 11.7%, and the quantum yield of NIR760-mbc94 is about 15.2%.

NIR760-mbc94 Has Low Toxicity to Living Cells. We used the CellTiter-Glo Luminescent Cell Viability Assay kit to evaluate cell toxicity. The assay uses a homogeneous method of determining the number of viable cells in culture based on a luminescent quantitation of the ATP present, an indicator of metabolically active cells. As shown in Figure 2, CB_2-mid DBT cells treated with NIR760-mbc94 exhibited a comparably low cytotoxicity to those treated with ICG, the only FDA approved NIR fluorescent dye. Tamoxifen, a commonly used chemotherapy drug, served as the positive control. As expected, the number of viable cells dramatically decreased after treatment with 50 and 100 μM tamoxifen.

RT-PCR and Western Blot. RT-PCR was performed using primers for the CB_2 receptor or GAPDH, with expected amplicons of 165 and 124 base pairs (bp), respectively. CB_2R-

dx.doi.org/10.1021/bc400328m | Bioconjugate Chem. 2013, 24, 1907−1916

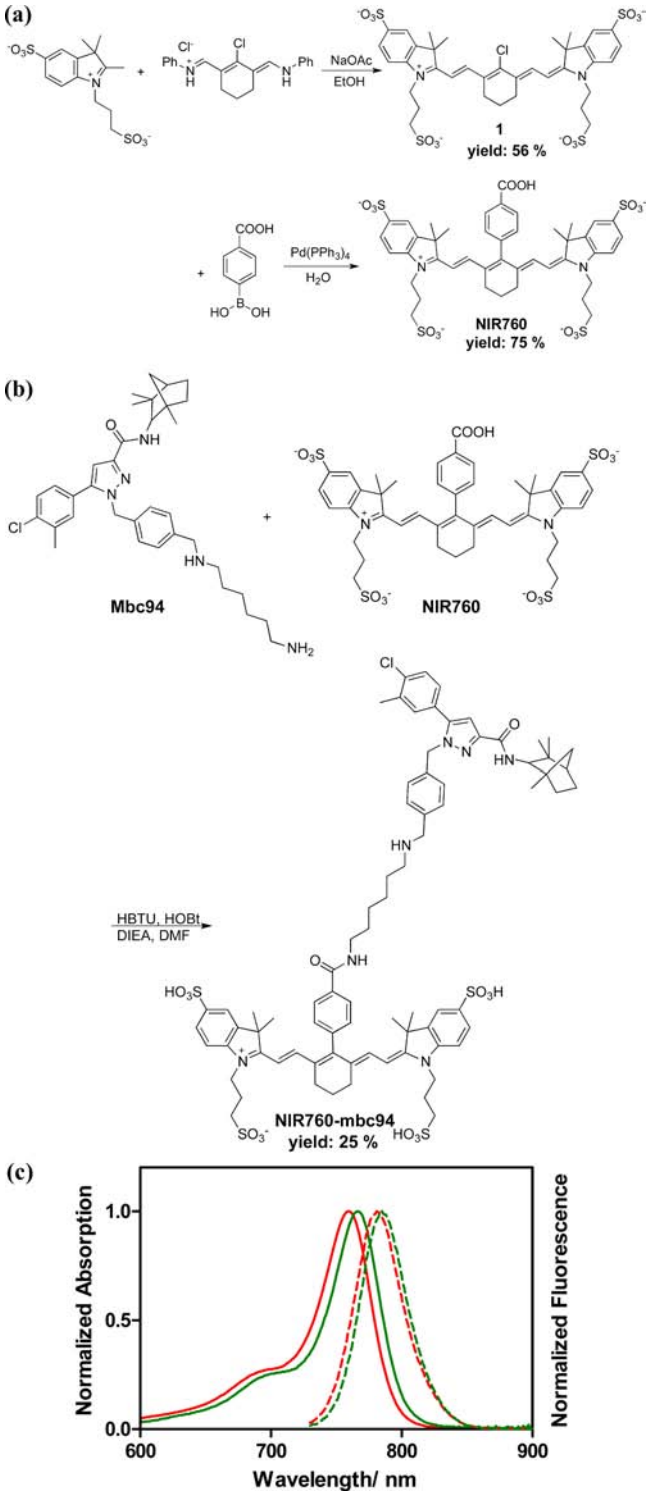

Figure 1. Synthesis and photophysical properties of NIR760-mbc94. (a, b) Synthesis of NIR760-mbc94. (c) Normalized UV−vis absorption (solid lines) and emission spectra (dotted lines) of NIR760 (red) and NIR760-mbc94 (green) in water at a concentration of 1×10^{-6} M (λ_{ex}= 720 nm).

positive bands at 165 bp were detected in both CB_2-mid DBT cells and tumors using RT-PCR (Figure 3a). GAPDH positive band at 124 bp were also found in CB_2-mid DBT cells and tumors samples. Therefore, CB_2-mid DBT cells and tumors revealed positive mRNA expression of CB_2R. In western blots of protein homogenates from CB_2-mid DBT cells and tumors,

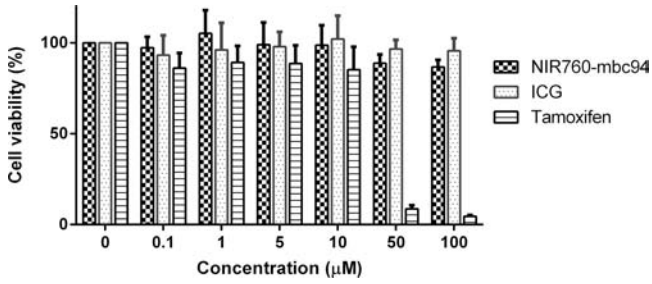

Figure 2. Cytotoxicity of NIR760-mbc94. To evaluate cytotoxicity of NIR760-mbc94, CB_2-mid DBT cells were incubated with 0, 0.1, 1, 5, 10, 50, or 100 μM of NIR760-mbc94 for 24 h. Cell viability was measured using the CellTilter-Glo Luminescent Cell Viability assay. Tamoxifen served as the positive control, and ICG served as the negative control. Each data point represents the mean ± SD based on triplicate samples.

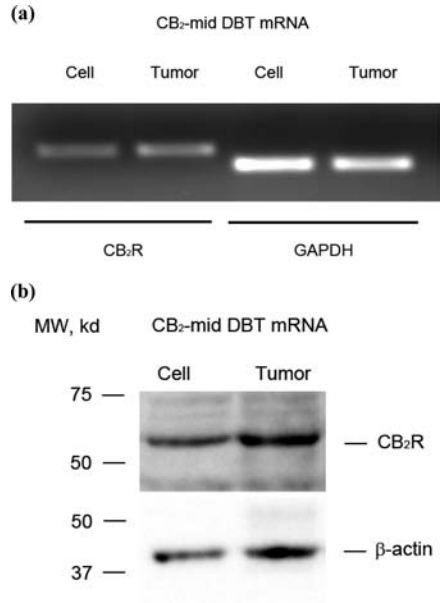

Figure 3. Expression of CB_2R in CB_2-mid DBT cells and tumor mRNA and total protein samples. (a) CB_2R expression at the mRNA level was assessed in CB_2-mid DBT cell lines and tumor tissue samples by RT-PCR. (b) CB_2R expression at the total protein level was assessed in CB_2-mid DBT cell lines and tumor tissue samples by western blot using a CB_2R monoclonal antibody.

we found major bands at 55 kDa, which indicated positive expression of CB_2R at the protein level. β-Actin (loading control)-positive bands at 42 kDa were also present in CB_2-mid DBT cells and tumor protein samples (Figure 3b).

NIR760-mbc94 Has Nanomolar Level Binding Affinity with CB_2R. To determine NIR760-mbc94's binding affinity to CB_2R in intact cells, we used an in vitro saturation binding assay to measure the equilibrium dissociation constant (K_d) and the maximum specific binding (B_{max}). A large excess of SR144528 was added to a parallel set of cells to saturate the receptor binding sites and to account for nonspecific binding. A representative saturation binding curve is shown in Figure 4. The data show that NIR760-mbc94 binds to CB_2R with a K_d of 26.9 nM (±3.7) and B_{max} of 259.8 pmol/mg (±11.9).

NIR760-mbc94 Specifically Binds to CB_2R in Vitro. To evaluate the specificity and imaging potential of NIR760-mbc94 in vitro, we incubated CB_2-mid DBT cells with 5 μM of NIR760-mbc94 or NIR760 at 37 °C for 30 min with or without

dx.doi.org/10.1021/bc400328m | Bioconjugate Chem. 2013, 24, 1907−1916

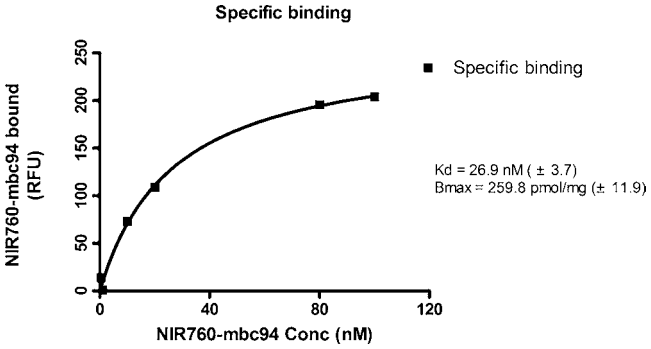

Figure 4. In vitro CB_2R saturation binding assay of NIR760-mbc94. CB_2-mid DBT cells were preincubated with or without 100 nM of the blocking agent SR144528 for 30 min and were then incubated for 1 h with an increasing concentration of NIR760-mbc94. Cells were then rinsed, and fluorescence at 790 nm was read with a Synergy H4 Hybrid Multi-Mode Microplate Reader. The specific binding was obtained by the subtraction of nonspecific binding from total binding. The dissociation constant (K_d) and receptor density (B_{max}) were estimated from the nonlinear fitting of the specific binding versus the concentration of NIR760-mbc94 using Prism software. Each data point represents the mean ± SD based on triplicate samples.

a 30 min pretreatment with 10 μM of SR144528, a well-known CB_2R ligand. After washing, no significant fluorescence signal was observed from cells incubated with the free dye (NIR760) control, whereas cells incubated with NIR760-mbc94 showed a strong fluorescence signal, primarily localized in cytoplasm. In addition, SR144528 significantly reduced NIR760-mbc94 uptake in CB_2-mid DBT cells (Figure 5a), indicating specific binding of NIR760-mbc94 to CB_2R. To evaluate quantitatively the specificity of NIR760-mbc94 for CB_2R, we performed CB_2-mid DBT cell binding assays using a multiwell plate reader system (Figure 5b). Cells incubated with NIR760-mbc94 showed a 4-fold higher fluorescence signal than those incubated with NIR760 (459.67 ± 27.54 vs 116.33 ± 15.37, $p < 0.001$). When challenged with SR144528 (10 μM), CB_2-mid DBT cells incubated with 5 μM of NIR760-mbc94 exhibited significantly lower (~40%) fluorescence intensity (from 459.67 ± 27.54 to 276.33 ± 57.62, $p = 0.008$), whereas NIR760- or vehicle (DMSO)-treated cells did not show a significant change in fluorescence intensity after the challenge.

In Vivo Tumor CB_2R-Targeted Optical Imaging with NIR760-mbc94. To study the potential of NIR760-mbc94 in CB_2R-targeted cancer imaging in living systems, in vivo optical imaging was performed in a CB_2-mid DBT mouse tumor model. In vivo imaging experiments were initiated approximately 10 days postinoculation of CB_2-mid DBT tumor cells subcutaneously. Mice were divided into three groups (three mice in each group): NIR760-mbc94 (10 nmol), free NIR760 (10 nmol), and 10-fold SR144528 (100 nmol) administered 1 h before NIR760-mbc94 (10 nmol) injection. The tumor sizes in all mice showed no significant difference (data not shown). Figure 6a shows the time-dependent fluorescence images of one representative mouse from each group. Because all images are displayed on the same scale, a direct visual comparison can be made among the tumor profiles of NIR760-mbc94, free NIR760 dye, and NIR760-mbc94 + SR144528. The free dye control mouse demonstrated an intense fluorescent signal throughout the whole body immediately after injection, but the strong signal only lasted for roughly 2 h. In addition, no obvious contrast enhancement in the tumor region was

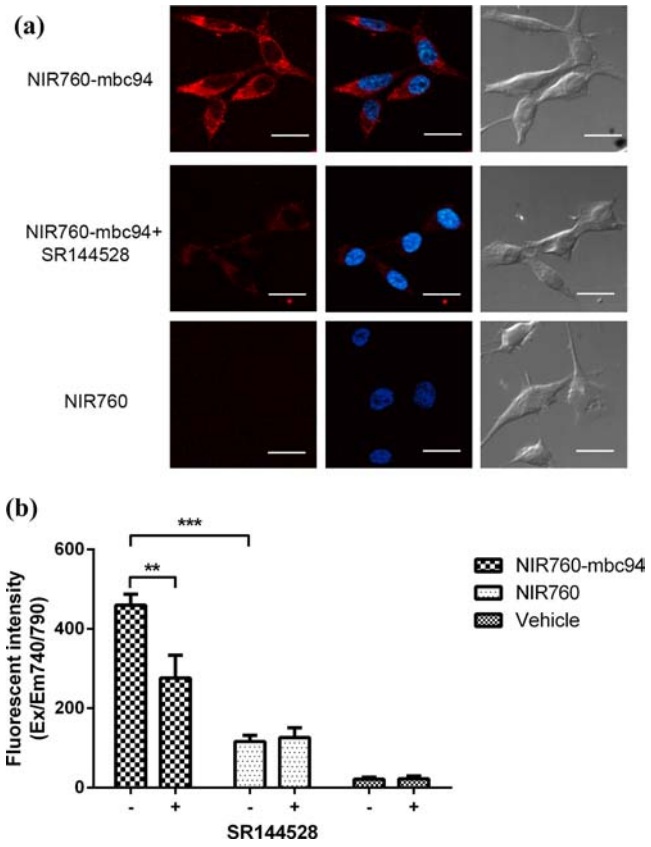

Figure 5. NIR760-mbc94 specifically binds to CB_2R in CB_2-mid DBT cells. CB_2-mid DBT cells were cultured for 24 h at 37 °C before imaging. CB_2-mid DBT cells were preincubated with or without 10 μM of blocking agent SR144528 for 30 min and were then incubated for 30 min with 5 μM of NIR760-mbc94 or free NIR760 or with DMSO as the vehicle. Cells were washed three times with serum-free medium. (a) Fluorescent cell imaging was obtained using Zeiss Axio Observer fluorescent microscopy with ApoTome 2 imaging system. From left to right: ICG filter (red), ICG filter (red) + DAPI filter (blue) merged, differential interference contrast (DIC). All fluorescence images are on the same scale. Scale bars = 20 μm. (b) Quantitative fluorescent signal was measured with a Synergy H4 Hybrid Multi-Mode Microplate Reader. Each data point represents the mean ± SD based on triplicate samples. (**$p < 0.01$ and ***$p < 0.001$).

observed. However, the tumor of the mouse injected with NIR760-mbc94 showed a visible signal contrast immediately after the injection, and the uptake gradually increased over time and reached maximum at 24 h postinjection. Tumor uptake gradually cleared 24 h postinjection, but the tumor contrast was visible even at 48 and 72 h postinjection. Mice treated with both NIR760-mbc94 and SR144528 showed less tumor uptake than NIR760-mbc94-treated mice at nearly all time points (Figure 6a).

To account for the nonspecific binding of NIR760-mbc94 in normal tissues, we normalized NIR760-mbc94 signals in the tumor area (T, right flank) with that in the normal area (N, same ROI in left flank) to generate time-dependent contrast enhancement (T/N) profiles (Figure 6b). In NIR760-treated mice, the peak T/N ratio appeared at 24 h postinjection, with only a 1.74-fold contrast enhancement, which gradually decreased to the baseline level at 72 h postinjection. By contrast, the T/N ratio of NIR760-mbc94-treated mice increased gradually over time, with a 2.04-, 2.86-, and 3.73-

dx.doi.org/10.1021/bc400328m | Bioconjugate Chem. 2013, 24, 1907−1916

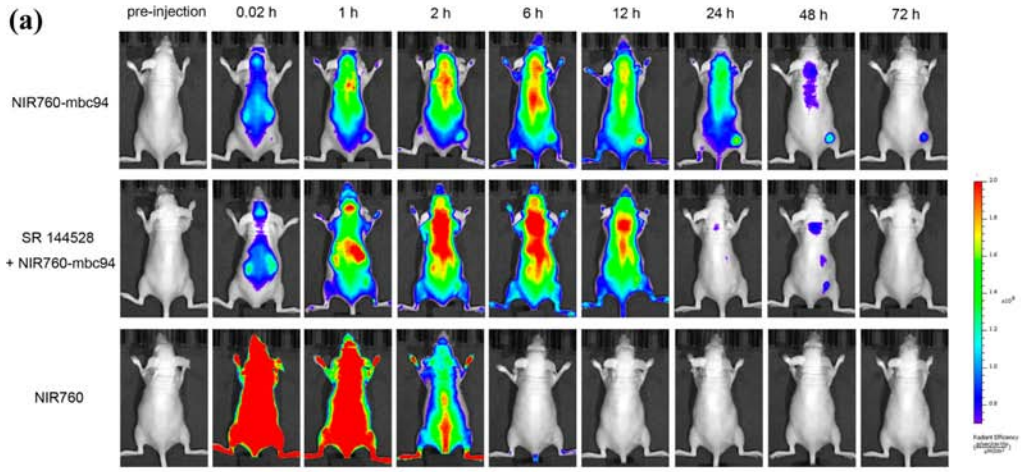

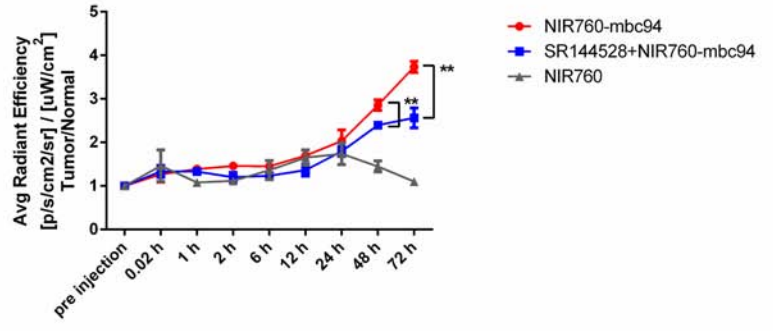

(c) **Tumor/Normal ratio**

Time points (hr)	NIR760 -mbc94	SR144528+ NIR760-mbc94	NIR760
0	1.00	1.00	1.00
0.02	1.27	1.33	1.46
1	1.39	1.33	1.08
2	1.46	1.20	1.12
6	1.45	1.23	1.36
12	1.70	1.36	1.65
24	2.04	1.80	1.74
48	2.86	2.40	1.45
72	3.73	2.56	1.10

Figure 6. In vivo tumor optical imaging and competitive blocking studies. To examine tumor CB_2R-targeted imaging, all mice were injected the following agents dissolved in 100 μL of saline via the tail vein: three received NIR760-mbc94, three received free NIR760, and three received SR144528 injected 1 h before NIR760-mbc94. (a) Mice were anesthetized and imaged with IVIS Lumina XR at preinjection and at 0.02, 1, 2, 6, 12, 24, 48, and 72 h postinjection. (b) Time activity curves of tumor/normal ratio among the NIR760-mbc94, free NIR760, and SR144528 + NIR760-mbc94 groups. The radiant efficiency of the tumor area at the right flank of the animal (T) and of the area at the left flank [normal tissue (N)] was calculated by the ROI function in the Living Image software. Dividing T by N yielded the contrast between the tumor tissue and the normal tissue (**$p < 0.01$). (c) Quantitative comparison of tumor-to-normal ratios among the NIR760-mbc94, free NIR760, and SR144528 + NIR760-mbc94 groups.

fold contrast enhancement at 24, 48, and 72 h postinjection, respectively. Importantly, challenged mice treated with both NIR760-mbc94 and SR144528 showed decreased T/N ratios as compared with unchallenged mice, with a 1.80-, 2.40-, and 2.56-fold contrast enhancement at 24, 48, and 72 h postinjection, respectively. A significant difference in the T/N ratio was found between challenged and unchallenged mice at the 48 (16% blockage effect, $p = 0.007$) and 72 h (31% blockage effect, $p = 0.001$) postinjection time points (Figure 6c). Similar to our in vitro competitive binding study, SR144528 partially inhibited tumor uptake of NIR760-mbc94 in vivo, indicating that NIR760-mbc94 labeled tumor tissues through specific binding to CB_2R.

Ex Vivo Imaging, Biodistribution, and Histological Study. After the last imaging data point, all CB_2-mid DBT tumor-bearing mice were sacrificed. The tumor and organs of interest (blood, heart, lung, liver, spleen, pancreas, kidney, muscle from left leg, and brain) were harvested and imaged with the IVIS imaging system (Figure 7a). The fluorescent intensities in the tumor and organs were measured, and the signal contrast (fluorescence signal from tumor or organ/signal from muscle) values are presented in Figure 7b,c. The NIR760-mbc94-treated mice showed an ex vivo T/N ratio as high as roughly 10 (9.77 ± 2.10), whereas SR144528-challenged mice showed a significantly lower T/N ratio of roughly 6 (6.32 ± 0.24 vs 9.77 ± 2.10, $p = 0.048$), and free dye control mice showed a T/N ratio of almost 1 (1.23 ± 0.16 vs 9.77 ± 2.10, $p < 0.001$). The significant signal contrast in the liver and kidney from unchallenged (liver/N = 12.53 ± 1.80 and kidney/N = 4.05 ± 0.92) and challenged (liver/N = 15.70 ± 2.35 and kidney/N = 6.10 ± 1.45) mice indicate that NIR760-mbc94 was cleared from both the liver and kidney. H&E staining (Figure 7d) from CB_2-mid DBT tumor tissues revealed that the tumor nuclei were irregular-shaped with hyperchromatin, polymorphism, and increased mitotic activity.

■ DISCUSSION

Targeting receptors that cancers overexpress remains a common strategy for molecular imaging of the disease. Examples of upregulated receptors include somatostatin, integrin, cholecystokinin-2, translocator protein, epidermal growth factor, human epidermal growth factor 2, vascular endothelial growth factor, folate, and estrogen receptors.[25]

dx.doi.org/10.1021/bc400328m | Bioconjugate Chem. 2013, 24, 1907−1916

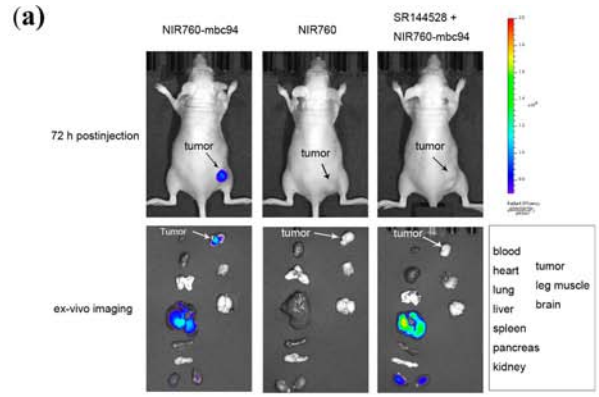

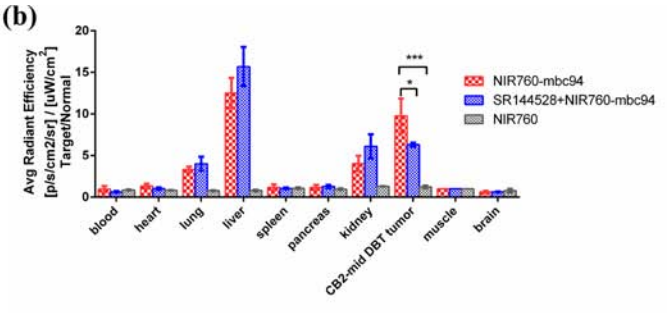

(c) **Target/Normal ratio**

Organs	NIR760-mbc94	SR144528+ NIR760-mbc94	NIR760
blood	0.97	0.63	0.86
heart	1.33	1.02	0.83
lung	3.32	4.01	0.77
liver	12.53	15.70	0.79
spleen	1.18	1.05	1.06
pancreas	1.16	1.28	0.96
kidney	4.05	6.10	1.30
tumor	9.77	6.32	1.23
muscle	1.00	1.00	1.00
brain	0.62	0.62	0.78

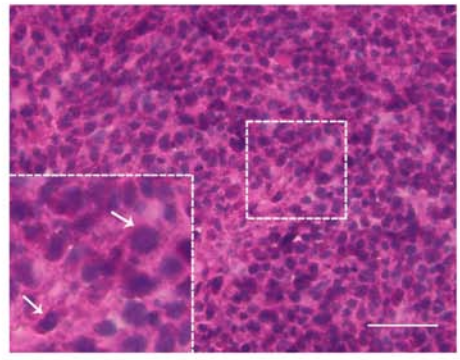

Figure 7. Ex vivo optical imaging, biodistribution, and histological study. (a) Ex vivo imaging of the tumor and selected organs 72 h postinjection of NIR760-mbc94, free NIR760, or SR144528 + NIR760-mbc94. (b) Graphical representation of target/normal contrast ratio for the ex vivo study among the NIR760-mbc94, free NIR760, and SR144528 + NIR760-mbc94 groups. (c) Quantitative comparison of target/normal ratios among the NIR760-mbc94, free NIR760, and SR144528 + NIR760-mbc94 groups (*p < 0.05 and ***p < 0.001). (d) Tumor samples were embedded in Tissue-Tek OCT compound mounting medium, frozen in liquid nitrogen, and cryostat-sectioned (5 μm). Histological sections from cryostat blocks were stained with H&E. Arrowheads show representative tumor nuclei that are irregularly shaped with hyperchromatin, polymorphism, and increased mitotic activity. Scale bar = 50 μm.

However, many of these receptors, although at lower levels, are expressed in normal tissues as well.[26−34] As a result, high-contrast imaging is challenging. CB_2R is a superior target for cancer-imaging studies. Under basal conditions, CB_2R is expressed mainly in cells of the immune system, and the expression in other types of cells is low to undetectable.[20,35] The high upregulation of CB_2R in certain cancer cells and the undetectable expression in corresponding normal tissues allows for high-contrast cancer imaging. In addition, CB_2R-targeted imaging could help to elucidate the exact role of CB_2R in cancer progression as well as its potential as a therapeutic target and could be applied to cancer diagnosis, therapeutic monitoring, and high-throughput drug screening.[20]

Among all imaging modalities, NIR optical imaging stands out as a promising and low-cost technique with high sensitivity and resolution. NIR optical imaging has been widely used to image cancer both in vitro and in vivo.[25] In our previous study, we developed the first NIR CB_2R-targeted probe, NIR-mbc94, and validated its selective binding to CB_2R in CB_2-mid DBT cells.[20] To advance the scope of our CB_2R-targeted NIR imaging probe to in vivo applications, we synthesized a novel CB_2R-targeted NIR probe, NIR760-mbc94, and investigated its potential in tumor CB_2R-targeted imaging both in vitro and in vivo. NIR-mbc94 and NIR760-mbc94 share the same targeting moiety, whereas the NIR fluorophores are different. IRDye-800CW, the fluorophore used in NIR-mbc94, is a commercially available dye with high hydrophilicity and intense absorption and emission in the desired NIR region. However, IRDye-800CW is a high-cost asymmetric dye whose synthesis and purification is rather challenging. In addition, previous studies indicate that heptamethine cyanine dyes with an enol ether linkage, such as IRDye-800CW, have significant stability issues.[21] NIR760 is a new NIR fluorescent dye developed in our lab with high hydrophilicity and intense NIR absorption and emission. Moreover, NIR760 is a symmetric dye that can be easily synthesized with low cost. Furthermore, NIR760 overcomes the stability issue of IRDye-800CW with a more robust C−C linkage at the meso position of the polymethine chain. The spectroscopic properties and overall reaction yields of NIR760 and IRDye-800CW are summarized in Table 1. NIR760 has a comparably high molar extinction coefficient (ε = 2.14 × 10^5 M^{-1} cm^{-1}) to that of IRDye-800CW (ε = 2.37 × 10^5 M^{-1} cm^{-1}),[36] and it has a significantly higher fluorescence quantum yield (Φ = 20.1 vs 14.2% for IRDye-800CW). In addition, NIR760 can be synthesized with only two steps and an overall yield of 42%, whereas the synthesis of IRDye-800CW

dx.doi.org/10.1021/bc400328m | Bioconjugate Chem. 2013, 24, 1907−1916

Table 1. Comparison of Spectroscopic Properties and Reaction Yield Between NIR760, IRDye-800CW, and ICG in FBS[a]

	λ_{abs} (nm)	ε (M^{-1} cm^{-1})	λ_{em} (nm)	Stokes shift (nm)	Φ (%)	yield
NIR760	766	2.14	785	19	20.1[b]	42%
IRDye-800CW	786	2.37	800	14	14.2	13%
ICG	807	1.21	822	15	9.3	

[a]Data from ref 36 was used for IRDye-800CW and ICG. [b]ICG was used as the standard.

(with terminal carboxylic acid group) requires four reaction steps with an overall yield of only 13%.[37] To compare the stability of these two dyes, we exposed two dye samples in PBS with the same initial absorption intensity to the ambient light and monitored the change of fluorescence intensity over time. As shown in Figure S1, after 2 h of exposure, the fluorescence intensity of IRDye-800CW decreased by 55%, whereas that of NIR760 decreased by only 37%. Overall, NIR760 appears to be a superior NIR dye. The attachment of the CB_2R targeting moiety (mbc94) red-shifted the maximum absorption of NIR760 from 760 to 766 nm (Figure 1b). NIR760-mbc94 has a high molar extinction coefficient (ε = 1.44 × 10^5 M^{-1} cm^{-1}) and strong emission at 785 nm with a quantum yield (Φ = 15.2% in water) that is more than 50 times higher than that of ICG (Φ = 0.28% in water[38]), the only FDA-approved NIR fluorescent dye.

NIR760-mbc94 specifically binds to CB_2R in vitro, as evidenced by studies from cell saturation binding assays, fluorescent microscopy, and a multiplate reader system. As shown in Figure 4, the K_d value for NIR760-mbc94 bound to CB_2R was 26.9 nM (±3.7) and the B_{max} over K_d value was roughly 10, indicating favorable binding affinity for in vivo imaging. Furthermore, cellular fluorescence imaging (Figure 5a) showed that NIR760-mbc94 was internalized and localized to the cytoplasm of CB_2-mid DBT cells and that SR144528 partially (40%) inhibited NIR760-mbc94 uptake. Cells treated with free dye control did not show significant fluorescence signal. These results indicate specific binding of NIR760-mbc94 to the target receptor and are consistent with our previous cellular imaging studies using another fluorescent CB_2R probe.[8,20,] As a more quantitative approach, a multiplate reader system was used to analyze cellular uptake of NIR760-mbc94 (Figure 5b). Cells treated with NIR760-mbc94 showed a 4-fold higher fluorescence signal than those with free NIR 760 dye (p < 0.001), and blocking with SR144528 (10 μM) resulted in an approximately 40% decrease in fluorescence intensity for cells with NIR760-mbc94 (p < 0.01).

Encouraged by the promising in vitro imaging results, we evaluated the CB_2R-targeted imaging potential of NIR760-mbc94 in CB_2-mid DBT tumor-bearing mice. Free NIR760 showed quick bioclearance from the bodies without tumor contrast, and no significant fluorescence signal was observed at 6 h postinjection. Conversely, we observed significant tumor contrast in the mice injected with NIR760-mbc94, and the T/N ratio increased gradually over time, with a 2.04-, 2.86-, and 3.73-fold of contrast enhancement at 24, 48, and 72 h postinjection, respectively. The high tumor uptake and slow clearance of NIR760-mbc94 may involve CB_2R specific binding as well as a rebound effect (GPCR can translocate from cytoplasm back to the cell surface after internalizing the ligand), which is a typical internalization mechanism observed in GPCRs.[39]

To validate further the CB_2R specificity of NIR760-mbc94 in vivo, the blocking effect was studied by injecting mice with blocking agent SR144528 1 h before the NIR760-mbc94 injection. We observed a 31% decrease in the T/N ratio at the 72 h postinjection time point (p < 0.05), which was consistent with the in vitro blocking study where 40% blocking was shown. The partial inhibition indicates nonspecific binding of NIR760-mbc94, which may result from its inherent net negative charge. Recent studies have shown that the nonspecific binding of imaging probes can be minimized by reducing the net charge.[40] Future study will involve the development of optimized CB_2R probes with reduced nonspecific binding to allow for enhanced imaging contrast at the target.

CONCLUSIONS

We have developed a novel CB_2R-targeted NIR probe that demonstrated specific binding both in vitro and in vivo. This study reports the first in vivo CB_2R-targeted optical imaging using a molecular probe. Given the important but unclear role of CB_2R in cancer progression and therapy, such a targeted probe may be of great value to the CB_2R and cancer research communities. Specifically, NIR760-mbc94 may have great potential for noninvasive diagnostic imaging of cancer, monitoring therapeutic effects, high-throughput screening of CB_2R ligands, and defining the relationship between CB_2R and cancer.

ASSOCIATED CONTENT

Supporting Information

Stability of NIR760 and IRDye-800CW in PBS. This material is available free of charge via the Internet at http://pubs.acs.org.

AUTHOR INFORMATION

Corresponding Author

*Phone: 412-624-2565. Fax: 412-624-2598. E-mail: baim@upmc.edu.

Author Contributions

‖These authors contributed equally.

Notes

The authors declare no competing financial interest.

ACKNOWLEDGMENTS

We thank Dr. Nephi Stella at the University of Washington for providing DBT cells and technical advice. We also thank Dr. Xiangqun Xie at the University of Pittsburgh for providing support to this project. This work was supported by the startup fund provided by the Department of Radiology, University of Pittsburgh. This project used the UPCI imaging facilities supported, in part, by award P30CA047904.

REFERENCES

(1) Rodriguez de Fonseca, F., Del Arco, I., Bermudez-Silva, F. J., Bilbao, A., Cippitelli, A., and Navarro, M. (2005) The endocannabinoid system: Physiology and pharmacology. *Alcohol Alcohol. 40*, 2−14.

(2) Munro, S., Thomas, K. L., and Abushaar, M. (1993) Molecular characterization of a peripheral receptor for cannabinoids. *Nature 365*, 61−65.

(3) Scotter, E. L., Abood, M. E., and Glass, M. (2010) The endocannabinoid system as a target for the treatment of neurodegenerative disease. *Br. J. Pharmacol. 160*, 480−98.

(4) Klein, T. W., Newton, C., Larsen, K., Lu, L., Perkins, I., Nong, L., and Friedman, H. (2003) The cannabinoid system and immune modulation. *J. Leukocyte Biol. 74*, 486−96.

(5) Velasco, G., Carracedo, A., Blazquez, C., Lorente, M., Aguado, T., Haro, A., Sanchez, C., Galve-Roperh, I., and Guzman, M. (2007) Cannabinoids and gliomas. *Mol. Neurobiol. 36*, 60−7.
(6) Pacher, P., Batkai, S., and Kunos, G. (2006) The endocannabinoid system as an emerging target of pharmacotherapy. *Pharmacol. Rev. 58*, 389−462.
(7) Galiegue, S., Mary, S., Marchand, J., Dussossoy, D., Carriere, D., Carayon, P., Bouaboula, M., Shire, D., Lefur, G., and Casellas, P. (1995) Expression of central and peripheral cannabinoid receptors in human immune tissues and leukocyte subpopulations. *Eur. J. Biochem. 232*, 54−61.
(8) Bai, M. F., Sexton, M., Stella, N., and Bornhop, D. J. (2008) MBC94, a conjugable ligand for cannabinoid CB2 receptor imaging. *Bioconjugate Chem. 19*, 988−992.
(9) Velasco, G., Sanchez, C., and Guzman, M. (2012) Towards the use of cannabinoids as antitumour agents. *Nat. Rev. Cancer 12*, 436−444.
(10) Blazquez, C., Carracedo, A., Barrado, L., Real, P. J., Fernandez-Luna, J. L., Velasco, G., Malumbres, M., and Guzman, M. (2006) Cannabinoid receptors as novel targets for the treatment of melanoma. *FASEB J. 20*, 2633−2635.
(11) Qamri, Z., Preet, A., Nasser, M. W., Bass, C. E., Leone, G., Barsky, S. H., and Ganju, R. K. (2009) Synthetic cannabinoid receptor agonists inhibit tumor growth and metastasis of breast cancer. *Mol. Cancer Ther. 8*, 3117−3129.
(12) Sarfaraz, S., Afaq, F., Adhami, V. M., Malik, A., and Mukhtar, H. (2006) Cannabinoid receptor agonist-induced apoptosis of human prostate cancer cells LNCaP proceeds through sustained activation of ERK1/2 leading to G1 cell cycle arrest. *J. Biol. Chem. 281*, 39480−39491.
(13) Xu, X., Liu, Y., Huang, S., Liu, G., Xie, C., Zhou, J., Fan, W., Li, Q., Wang, Q., Zhong, D., and Miao, X. (2006) Overexpression of cannabinoid receptors CB1 and CB2 correlates with improved prognosis of patients with hepatocellular carcinoma. *Cancer Genet. Cytogenet. 171*, 31−38.
(14) Evens, N., Bosier, B., Lavey, B. J., Kozlowski, J. A., Vermaelen, P., Baudemprez, L., Busson, R., Lambert, D. M., Van Laere, K., Verbruggen, A. M., and Bormans, G. M. (2008) Labelling and biological evaluation of [(11)C]methoxy-Sch225336: A radioligand for the cannabinoid-type 2 receptor. *Nucl. Med. Biol. 35*, 793−800.
(15) Evens, N., Muccioli, G. G., Houbrechts, N., Lambert, D. M., Verbruggen, A. M., Van Laere, K., and Bormans, G. M. (2009) Synthesis and biological evaluation of carbon-11- and fluorine-18-labeled 2-oxoquinoline derivatives for type 2 cannabinoid receptor positron emission tomography imaging. *Nucl. Med. Biol. 36*, 455−465.
(16) Gao, M., Wang, M., Miller, K. D., Hutchins, G. D., and Zheng, Q. H. (2010) Synthesis and in vitro biological evaluation of carbon-11-labeled quinoline derivatives as new candidate PET radioligands for cannabinoid CB2 receptor imaging. *Bioorg. Med. Chem. 18*, 2099−2106.
(17) Turkman, N., Shavrin, A., Paolillo, V., Yeh, H. H., Flores, L., Soghomonian, S., Rabinovich, B., Volgin, A., Gelovani, J., and Alauddin, M. (2012) Synthesis and preliminary evaluation of [18F]-labeled 2-oxoquinoline derivatives for PET imaging of cannabinoid CB2 receptor. *Nucl. Med. Biol. 39*, 593−600.
(18) Evens, N., and Bormans, G. M. (2010) Non-invasive imaging of the type 2 cannabinoid receptor, focus on positron emission tomography. *Curr. Top. Med. Chem. 10*, 1527−1543.
(19) Escobedo, J. O., Rusin, O., Lim, S., and Strongin, R. M. (2010) NIR dyes for bioimaging applications. *Curr. Opin. Chem. Biol. 14*, 64−70.
(20) Sexton, M., Woodruff, G., Horne, E. A., Lin, Y. H., Muccioli, G. G., Bai, M., Stern, E., Bornhop, D. J., and Stella, N. (2011) NIR-mbc94, a fluorescent ligand that binds to endogenous CB(2) receptors and is amenable to high-throughput screening. *Chem. Biol. 18*, 563−568.
(21) Lee, H., Mason, J. C., and Achilefu, S. (2006) Heptamethine cyanine dyes with a robust C−C bond at the central position of the chromophore. *J. Org. Chem. 71*, 7862−7865.
(22) Cudaback, E., Marrs, W., Moeller, T., and Stella, N. (2010) The expression level of CB1 and CB2 receptors determines their efficacy at inducing apoptosis in astrocytomas. *PLoS One 5*, e8702-1−e8702-10.
(23) Cowell, L. N., Graham, J. D., Bouton, A. H., Clarke, C. L., and O'Neill, G. M. (2006) Tamoxifen treatment promotes phosphorylation of the adhesion molecules, p130Cas/BCAR1, FAK and Src, via an adhesion-dependent pathway. *Oncogene 25*, 7597−7607.
(24) Sexton, M., Woodruff, G., Cudaback, E., Kreitzer, F. R., Xu, C., Lin, Y. H., Moller, T., Bai, M., Manning, H. C., Bornhop, D., and Stella, N. (2009) Binding of NIR-conPK and NIR-6T to astrocytomas and microglial cells: Evidence for a protein related to TSPO. *PLos One 4*, e8271-1−e8271-9.
(25) Bai, M., and Bornhop, D. J. (2012) Recent advances in receptor-targeted fluorescent probes for in vivo cancer imaging. *Curr. Med. Chem. 19*, 4742−4758.
(26) Hu, R., Dawood, S., Holmes, M. D., Collins, L. C., Schnitt, S. J., Cole, K., Marotti, J. D., Hankinson, S. E., Colditz, G. A., and Tamimi, R. M. (2011) Androgen receptor expression and breast cancer survival in postmenopausal women. *Clin. Cancer Res. 17*, 1867−1874.
(27) Reubi, J. C., Waser, B., Gugger, M., Friess, H., Kleeff, J., Kayed, H., Buchler, M. W., and Laissue, J. A. (2003) Distribution of CCK1 and CCK2 receptors in normal and diseased human pancreatic tissue. *Gastroenterology 125*, 98−106.
(28) Chrysogelos, S. A., and Dickson, R. B. (1994) EGF receptor expression, regulation, and function in breast cancer. *Breast Cancer Res. Treat. 29*, 29−40.
(29) Yang, X. R., Figueroa, J. D., Hewitt, S. M., Falk, R. T., Pfeiffer, R. M., Lissowska, J., Peplonska, B., Brinton, L. A., Garcia-Closas, M., and Sherman, M. E. (2012) Estrogen receptor and progesterone receptor expression in normal terminal duct lobular units surrounding invasive breast cancer. *Breast Cancer Res. Treat. 137*, 837−847.
(30) Buxant, F., Engohan-Aloghe, C., and Noel, J. C. (2010) Estrogen receptor, progesterone receptor, and glucocorticoid receptor expression in normal breast tissue, breast in situ carcinoma, and invasive breast cancer. *Appl. Immunohistochem. Mol. Morphol. 18*, 254−257.
(31) Parker, N., Turk, M. J., Westrick, E., Lewis, J. D., Low, P. S., and Leamon, C. P. (2005) Folate receptor expression in carcinomas and normal tissues determined by a quantitative radioligand binding assay. *Anal. Biochem. 338*, 284−293.
(32) Gebre-Medhin, M., Kindblom, L. G., Wennbo, H., Tornell, J., and Meis-Kindblom, J. M. (2001) Growth hormone receptor is expressed in human breast cancer. *Am. J. Pathol. 158*, 1217−1222.
(33) Anholt, R. R. H., Pedersen, P. L., Desouza, E. B., and Snyder, S. H. (1986) The peripheral-type benzodiazepine receptor - localization to the mitochondrial outer-membrane. *J. Biol. Chem. 261*, 576−583.
(34) Laws, S. A. M., Gough, A. C., Evans, A. A., Bains, M. A., and Primrose, J. N. (1997) Somatostatin receptor subtype mRNA expression in human colorectal cancer and normal colonic mucosae. *Br. J. Cancer 75*, 360−366.
(35) Munro, S., Thomas, K. L., and Abu-Shaar, M. (1993) Molecular characterization of a peripheral receptor for cannabinoids. *Nature 365*, 61−5.
(36) Choi, H. S., Nasr, K., Alyabyev, S., Feith, D., Lee, J. H., Kim, S. H., Ashitate, Y., Hyun, H., Patonay, G., Strekowski, L., Henary, M., and Frangioni, J. V. (2011) Synthesis and in vivo fate of zwitterionic near-infrared fluorophores. *Angew. Chem., Int. Ed. 50*, 6258−6263.
(37) Lugade, A. G., Narayanan, N. W. M. A., and Draney, D. (2006) U.S. Patent 2006/0063247 A1.
(38) Benson, R. C., and Kues, H. A. (1978) Fluorescence properties of indocyanine green as related to angiography. *Phys. Med. Biol. 23*, 159−163.
(39) Gao, B., Curtis, T. M., Blumenstock, F. A., Minnear, F. L., and Saba, T. M. (2000) Increased recycling of (alpha)5(beta)1 integrins by lung endothelial cells in response to tumor necrosis factor. *J. Cell. Sci. 113*, 247−257.
(40) Achilefu, S., Bloch, S., Markiewicz, M. A., Zhong, T., Ye, Y., Dorshow, R. B., Chance, B., and Liang, K. (2005) Synergistic effects of

light-emitting probes and peptides for targeting and monitoring integrin expression. *Proc. Natl. Acad. Sci. U.S.A. 102*, 7976−7981.